Single-particle strength in neutron-rich ^{69}Cu from the ^{70}Zn(d, ^{3}He)^{69}Cu proton pick-up reaction

P. Morfouace,[1] S. Franchoo,[1] K. Sieja,[2] I. Stefan,[1] N. de Séréville,[1] F. Hammache,[1] M. Assié,[1] F. Azaiez,[1] C. Borcea,[3] R. Borcea,[3] L. Grassi,[4] J. Guillot,[1] B. Le Crom,[1] L. Lefebvre,[1] I. Matea,[1] D. Mengoni,[5] D. Napoli,[6] C. Petrone,[3] M. Stanoiu,[3] D. Suzuki,[1] and D. Testov[1]

[1]*Institut de Physique Nucléaire et Université Paris-Sud, 91406 Orsay Cedex, France*
[2]*Université de Strasbourg, IPHC, CNRS, UMR7178, 67037 Strasbourg, France*
[3]*Institute of Atomic Physics, IFIN-HH, Bucharest-Mağurele, P.O. Box MG6, Romania*
[4]*Ruder Bošković Institute, Bijenička 54, 10000 Zagreb, Croatia*
[5]*Dipartimento di Fisica e Astronomia dell'Università and INFN, 35131 Padova, Italy*
[6]*INFN Laboratori Nazionali di Legnaro, 35020 Legnaro (Pd), Italy*

(Received 7 March 2016; published 7 June 2016)

We have performed the ^{70}Zn(d,^{3}He)^{69}Cu proton pick-up reaction in direct kinematics using a deuteron beam at 27 MeV. The outgoing ^{3}He particles were detected at the focal-plane detection system of an Enge split-pole spectrometer. The excitation-energy spectrum was reconstructed up to 7 MeV and spectroscopic factors were obtained after analysis of the angular distributions in the finite-range distorted-wave Born approximation. The results show three new angular distributions for which the $\pi f_{7/2}$ strength was measured and a lower limit of the centroid is established. State-of-the-art shell-model calculations are performed and predict a $\pi f_{7/2}$ strength that lies too high in energy in comparison to our experimental results.

DOI: 10.1103/PhysRevC.93.064308

I. INTRODUCTION

The development of the shell-model by Mayer, Haxel, Suess, and Jensen [1,2] in 1949 still accounts for much of our understanding in nuclear structure at low excitation energy. It gives a description of the observed shell gaps at nucleon number equal to one of the so-called magic numbers: 2, 8, 20, 28, 50, 82, and 126. It is of great interest nowadays to study the evolution of the single-particle states around shell closures when moving far from stability. The understanding of this evolution is crucial to constrain the nucleon-nucleon interaction and the nuclear models. It is well established that magic numbers evolve when one moves away from stability [3]. One can wonder about the evolution of the $Z = 28$ proton gap in neutron-rich isotope toward the key nucleus ^{78}Ni and especially between $N = 40$ and $N = 50$ with the filling of the $\nu g_{9/2}$ orbital. Very recently experimental results indicated a doubly magic ^{78}Ni by studying β-decay half-lives in its vicinity [4]. However it seems important to understand well the evolution of the $Z = 28$ proton gap that corresponds to the energy difference between the $\pi f_{7/2}$ orbital and the $\pi p_{3/2}$ or $\pi f_{5/2}$ orbitals. The behaviors of those orbitals will give a constraint on the πf-$\nu g_{9/2}$ proton-neutron interaction and it will allow us to test the strength of the tensor interaction and determine the spin-orbit splitting in this region. But to be able to constrain the gap evolution between $N = 40$ and $N = 50$, one needs to first determine the shell gap at $N = 40$, or the energy spacing between the $\pi f_{7/2}$ and the $\pi p_{3/2}$ orbital.

To probe the proton gap, the neutron-rich Cu isotopes are good candidates since they are composed of one proton outside a nickel core. In this article we propose to determine the proton gap in ^{69}Cu at $N = 40$. Indeed this isotope is a crucial starting point to see the evolution of the orbitals in more neutron-rich copper isotopes. Moreover the $N = 40$ region gives rise to a lot of experiments and theoretical work where the existence of a subshell was acknowledged [5]. More recently the unexpected small experimental $B(E2; 0_1^+ \rightarrow 2_1^+)$ value was interpreted as an erosion of $N = 40$ and shows the importance of the proton core excitations in the ^{68}Ni nucleus [6,7]. Many investigations have been performed since, revealing a third 0^+ state at 2511 keV [8] while the second 0^+ state was readjusted at 1604 keV [9], this value is consistent with more recent studies [10,11]. This leads to a richer interpretation in a shell model-model approach and in a Monte Carlo shell model (MCSM) of a shape coexistence in ^{68}Ni with a spherical ground state 0_1^+ and two deformed states: a 0_2^+ oblate and 0_3^+ prolate one [12,13].

It is known from the β decay of the neutron-rich Ni isotopes that the first $5/2^-$ excited state in ^{63,65,67,69}Cu remains between 1 and 1.2 MeV while it drops very rapidly at 534 keV in ^{71}Cu and 166 keV in ^{73}Cu [14]. The sudden energy shift arises above $N = 40$ with the filling of neutrons in the $\nu g_{9/2}$ orbital. A spin inversion between $3/2^-$ and $5/2^-$ was even observed in ^{75}Cu for the ground state [15]. From the Coulomb excitation of neutron-rich Cu isotopes we also see a strong reduction of the $B(E2)$ value for the transition to the $3/2^-$ ground state $(5/2^- \rightarrow 3/2^-_{\text{g.s.}})$ in ^{69,71,73}Cu around 3.0 to 4.4 W.u. while it has a value between 16 and 12.5 W.u. for ^{63,65,67}Cu. The low value of $B(E2)$ indicates a single-particle character of the $5/2^-$ states from $N = 40$ to at least $N = 44$ and one can link its energy shift to the position of the $\pi f_{5/2}$ orbital going down when adding a neutron in the $\nu g_{9/2}$ orbital. This suggests a strong attractive $\pi f_{5/2}$-$\nu g_{9/2}$ interaction. With all those experimental observations, one can naturally wonder about the behavior of the $\pi f_{7/2}$ spin-orbit partner.

In the present work we extract the spectroscopic factors of the $7/2^-$ levels in ^{69}Cu with the aim to obtain the $\pi f_{7/2}$ strength function at $N = 40$ and serve as a reference for the other more exotic Cu isotopes. We choose to do so using the ^{70}Zn(d,^{3}He)^{69}Cu proton pick-up reaction, which gives precisely access to the proton-hole states in ^{69}Cu. This reaction was already performed by Zeidman and Nolen

using a deuteron beam of 23.3 MeV [16]. In that experiment angular distributions were obtained for five peaks: the $3/2^-$ ground state, $1/2^-$ at 1.11 MeV, $5/2^-$ at 1.23 and two $7/2^-$ states at 1.74 and 1.87 MeV, respectively. The $5/2^-$ state shows a surprisingly high spectroscopic factor ($C^2S = 1.5$) and is larger than in ^{63,65,67}Cu, therefore the authors assume a probable $5/2^-$,$7/2^-$ doublet near 1.23 MeV. The sum of spectroscopic factors in the p-$f_{5/2}$ orbitals gives 3.36 while one expects naively only two protons in those orbitals in Zn isotopes. The sum of the $7/2^-$ gives a total of 3.15 protons that represents only 39.3% of the $\pi f_{7/2}$ strength. If one assumes a doublet at 1.23 MeV where a $5/2^-$ exhibits a spectroscopic factor of the order of 0.5 like in the other Cu isotopes, then the number of protons in the p-$f_{5/2}$ orbitals sums to 2.36, this is closer to the value we expect. Moreover the low-lying ^{69}Cu states were also populated from the $(\vec{t},\alpha)$ experiment using a polarized triton beam of 17 MeV [17]. Because of the polarized triton one should be able to differentiate between a $5/2^-$ and $7/2^-$ state since the analyzing power A_y has a completely different shape for two different spins. For the peak at 1.21 MeV, a $L = 3$ state is clearly assigned but the experimental A_y is not reproduced either by the $5/2^-$ or $7/2^-$ distribution. They conclude that it corresponds to two unresolved states and give a spectroscopic factor of 1.2 that corresponds to a $5/2^-$ state at this energy. Concerning the other states, they are in fair agreement with Zeidman and Nolen. The only strong difference is the value of the spectroscopic factor for the $7/2^-$ state at 1.71 MeV, which differs from 33% between these two experiments. Concerning states around 1.21 MeV from more recent works, a $5/2^-$ state was seen at 1.214 MeV and a $3/2^-$ state at 1.298 MeV from β decay [14] but no other state that could correspond to a $7/2^-$ level was observed.

In order to well establish the centroid of the $\pi f_{7/2}$ strength distribution it seems necessary to measure the complementary $7/2^-$ states at higher excitation energy by extracting the spectroscopic factor of every fragment. In several recent papers it has been pointed out that spectroscopic factors are not true observables [18,19]. Nevertheless it was shown that in a set of coherent parametrization, spectroscopic factors provide a valuable and consistent information on the nuclear structure [20,21]. In this article, we aim to use a set of a coherent parametrization to define the $\pi f_{7/2}$ centroid in ^{69}Cu at $N = 40$. It serves as reference for more exotic Cu isotopes [22] in order to establish the behavior of the $\pi f_{7/2}$ strength with the adding of neutrons in the $\nu g_{9/2}$ orbital. Moreover because of the $N = 40$ subshell gap, the correlations are minimized in ^{69}Cu, thus this nucleus is an essential test for shell-model calculation in order to constrain the position of single-particle orbitals (or proton-neutron monopole interaction).

II. EXPERIMENT

The ^{70}Zn$(d,^3$He$)^{69}$Cu reaction was studied at the Alto facility at Orsay, France. A deuteron beam of about 200 nA was produced by the duoplasmatron ion source and accelerated by the 15 MV tandem to an energy of 27 MeV. The beam was transported to the target located at the object focal point of an Enge split-pole magnetic spectrometer [24]. An enriched ^{70}Zn target with a thickness of 18.7(9) μg/cm^2 on a backing

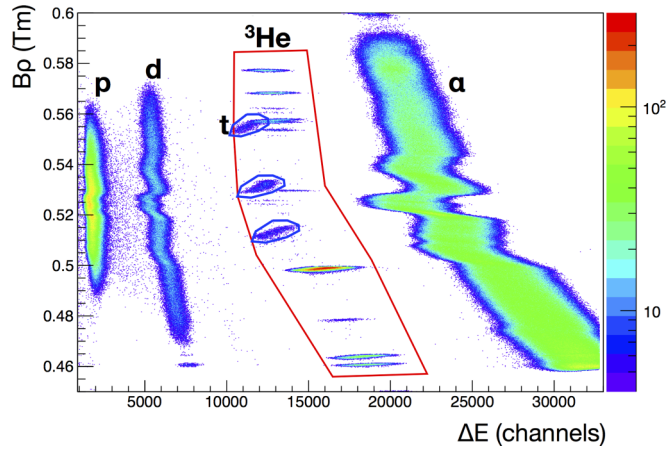

FIG. 1. Particle identification spectrum (magnetic rigidity versus energy loss) obtained with the focal-plane detector. The red contour indicates the $A = 3$ particles. All horizontal lines inside the red contour correspond to ^{3}He. The groups circled in blue correspond to tritons.

of carbon was used. The target thickness was determined through the Rutherford backscattering of α particles at the CSNSM, Orsay, France. With this method we could achieve an accuracy of 5% for the target thickness. The light charged particles from the reaction entered the split-pole spectrometer through a rectangular aperture covering a 1.16 msr solid angle, and were momentum analyzed and focused on the focal-plane detection system [25] as it is described in Ref. [26]. It consists of a 50 cm long position-sensitive proportional counter that gives the position of the particle, which is proportional to the magnetic rigidity $B\rho$. The position information is given by the time difference between the two sides of the delay line. A second detector is a proportional gas counter that provides a ΔE that corresponds to the energy loss in the gas. The gas used in the detector is isobutane at a pressure of 300 mbar. Finally, behind the position detector, there is a plastic scintillator measuring the residual energy of the particle. The active area of this plastic is smaller than the position detector reducing he achievable range of excitation energy for the residual nucleus. That is why, no condition on the plastic is applied in order not to reduce the excitation energy area. Particle identification was achieved through energy loss versus magnetic rigidity measurement as one can see in Fig. 1. The different masses are well identified, although with this method the triton and the ^{3}He are not well separated. Nevertheless the position of the focal-plane detection system was set up for our $(d,^3$He$)$ reaction of interest while the (d,t) reaction has a very different kinematics: the slope of the (d,t) reaction is much larger than the $(d,^3$He$)$ one. That is why the triton peaks are broad and their contribution will be easily identified in the final spectrum. Moreover the tritons we detect correspond only to the ^{12}C$(d,t)^{11}$C reaction that populates states in ^{11}C around 8 MeV of excitation energy.

After selection, the excitation-energy spectrum of ^{69}Cu was obtained. Angular distribution measurements were performed at spectrometer angles of 6°,9°,12°,15°,18°,21°, and 24°. The elastic scattering measurement was done at two other

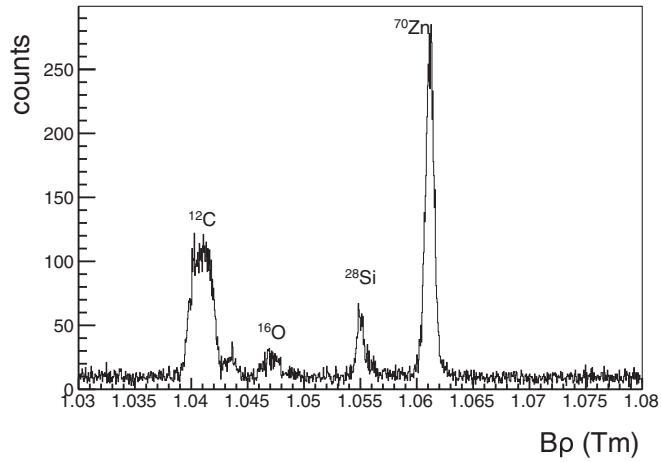

FIG. 2. Measured magnetic rigidity $B\rho$ for the elastic scattering of the deuteron on the target at $\theta_{\rm lab} = 40^\circ$.

angles of 30° and 40°. For each angle the position of the focal-plane detection system was adjusted to take into account the kinematic displacement and to have the final resolution as good as possible. With a unique setting of the magnetic field we measured the excitation-energy spectrum of ^{69}Cu up to 7 MeV with an average resolution for the excited states of $\sigma = 18(2)$ keV. Finally in order to measure the incident deuteron beam intensity we have used a Faraday cup at zero degree, which was performed with one current integrator.

III. DATA ANALYSIS AND RESULTS

A. Excitation-energy spectrum and peak identification

To quantify all the elements present in the target, elastic scattering at a large angle of 40° was measured in order to well spread the different elements. Besides ^{70}Zn and ^{12}C, the elastic scattering shows clearly the presence of ^{28}Si and ^{16}O as one can see in Fig. 2 where the magnetic rigidity of the scattered deuteron is displayed. The different peaks confirm the presence of different elements in the target. One can note that the resolution is degrading from zinc to carbon. This is due to the different slopes of the kinematic lines and in this run the kinematic displacement was adjusted for the ^{70}Zn(d,d) reaction. A $B\rho$ calibration of the focal-plane detector was performed using the elastic scattering with the different elements present in the target: ^{70}Zn, ^{28}Si, ^{16}O, and ^{12}C. The ground state of ^{11}B strongly populated from the well known ^{12}C$(d,^3$He$)^{11}$B reaction was also chosen for the calibration, in which the energy loss in the target was taken into account.

The $(d,^3$He) pick-up reaction with all the elements will populate discrete states in our excitation-energy window that one has to carefully identify in the final spectrum. As mentioned earlier, tritons and ^{3}He are not well separated, that is why the (d,t) reaction will also be a contamination in our spectrum. Nevertheless in our set of magnetic field, only the ^{12}C$(d,t)^{11}$C will populate discrete state in our spectrum and because of the very different kinematics they are easily identified as one can see in Fig. 3 where the excitation-energy spectrum of ^{69}Cu at $\theta_{\rm lab} = 21^\circ$ is shown. The other (d,t) reactions are situated in the continuum and can give a continuum flat background.

In Fig. 3, one can see that eight states have been populated and identified in ^{69}Cu at an energy of 0, 1.11, 1.23, 1.71, 1.87, 3.35, 3.70, and 3.94 MeV. For each of these peaks a Gaussian plus linear background fit was performed to determine the integral peak by peak at each angle to deduce the angular distributions. For all of these peaks, an average width of $\sigma = 18(2)$ keV is obtained and no peak are broader. From this work there is no evidence of a broader peak at 1.23 MeV so it seems that there is no doublet as it was suggested by previous works [16,17].

B. Angular distributions

In order to constrain the input parameters for the DWBA calculation but also to check the normalization procedure, the elastic scattering at eight different angles was measured. At each measured angle, the elastic peak was integrated and a careful normalization was performed by taking into account

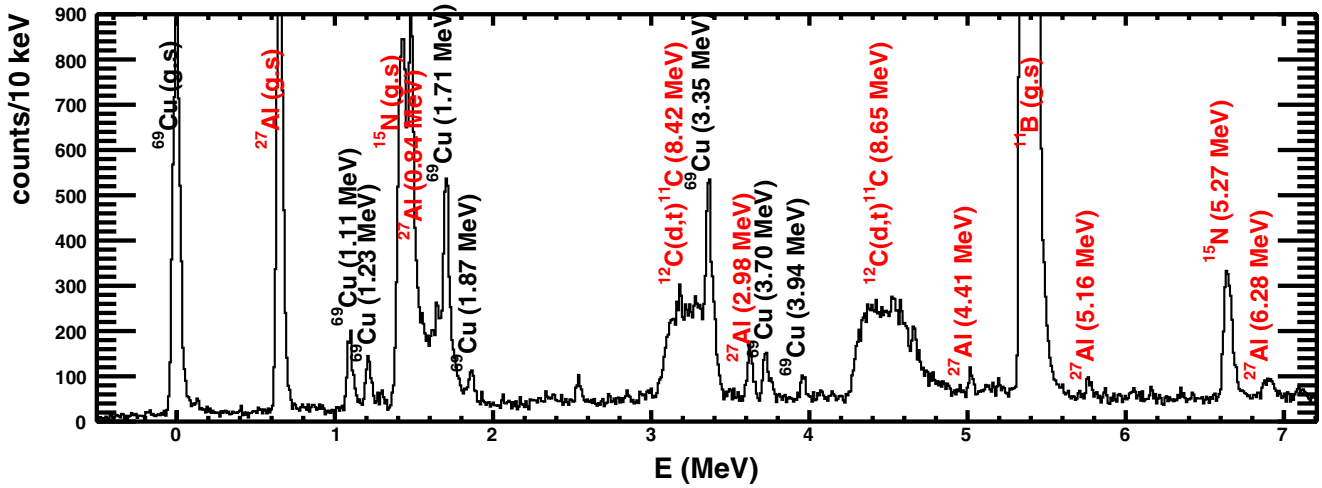

FIG. 3. Reconstructed excitation-energy spectrum of ^{69}Cu at $\theta_{\rm lab} = 21^\circ$ from the ^{70}Zn$(d,^3$He$)^{69}$Cu kinematics after gating on the $A = 3$ light charged particles.

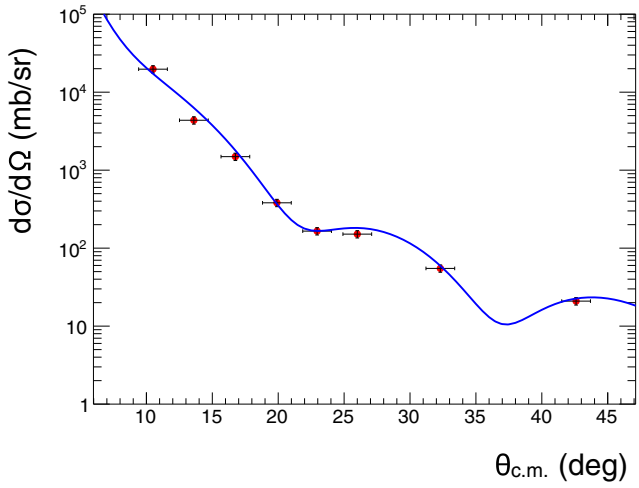

FIG. 4. Angular distribution of the elastic scattering for ^{70}Zn (red points) with the calculation where the Daehnick-F optical potential was used [28] (blue line).

the accumulated charges (beam intensity multiplied by the duration of the run), the target thickness, the aperture of the spectrometer and the Jacobian of the reaction for each excited states. In Fig. 4, the angular distribution of the elastic scattering is displayed together with the calculation. We have a good agreement between the experimental points and the calculation where the Daehnick-F optical potential was used [28], no scaling of the data has been done on top of the normalization, giving confidence in the normalization and in the input parameters used for the DWBA calculation as well. The Daehnick-L potential has been used for comparison in our previous study about ^{71}Cu [22], however this potential was not able to reproduce the data while the Daehnick-F reproduces well the elastic scattering (see Fig. 5 in Ref. [23]). To be consistent with our previous study, we decided to use the same optical potential for the ^{69}Cu case where we also observe a very good agreement between the experimental data and the calculation.

The same procedure was followed to extract the angular distributions for the populated states in ^{69}Cu. In a first step the distorted-wave Born approximation (DWBA) calculations were made in a similar way to those in Ref. [16] using the zero-range framework with the DWUCK-4 code [27] and the same bound-state parameters as in that paper ($r_0 = 1.20$ fm and $a_0 = 0.70$ fm), in such a way that direct comparisons could be made. For the incoming channel, the Daehnick-F optical potential was used [28], which reproduces well the angular distribution of the elastic scattering. For the outgoing channel, we used the Perey and Perey parametrization [29]. The second set of calculations were identical to the first, except that we adopted the commonly used bound-state parameters ($r_0 = 1.25$ fm and $a_0 = 0.65$). Finally a third set of calculations was performed in a finite-range framework using the DWUCK-5 finite-range code [30] and we used the Brida potential for the overlap between the deuteron and the ^{3}He particle [31]. In Fig. 5 we display the experimental angular distributions together with the DWBA calculations. The results of these calculations are listed in Table I. The errors given for our work correspond to the statistical ones.

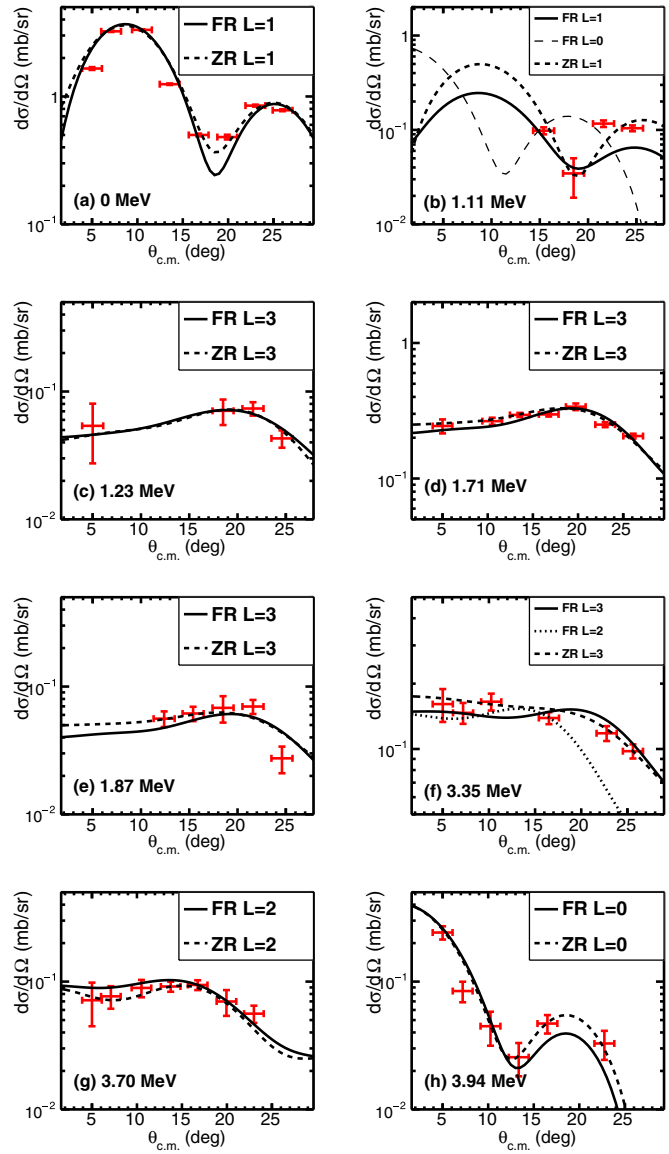

FIG. 5. Angular distributions of the states at 0 MeV (a), 1.11 MeV (b), 1.23 MeV (c), 1.71 MeV (d), 1.87 MeV (e), 3.35 MeV (f), 3.70 MeV (g), and 3.94 MeV (h). Both zero-range and finite-range calculations are shown.

As one can see in the first part of Table I where we use $r_0 = 1.20$ and $a_0 = 0.70$ fm and the zero-range DWBA calculation, our results are in fair agreement (within 25%) with the ones of Ref. [16] for the $3/2^-$ ground state and for the two $7/2^-$ excited states at 1.71 and 1.87 MeV. Our reported values are closer to the one from Ref. [16], except for the state at 1.87 MeV where the value is closer to Ref. [17]. For the $5/2^-$ state at 1.23 MeV we have a discrepancy of 40% between our values and the one from Ref. [16]. In this work we obtain a smaller value for the spectroscopic factor and the peak is as broad as the other one. This suggests that there is no doublet and that there is only one state located at 1.23 MeV, which is consistent from the β-decay experiment [14] where no other γ transition was observed around this energy. For the state at 1.11 MeV the contamination was very important for most of

TABLE I. Position in energy of the different populated states in ^{69}Cu, the transferred angular momentum L, the spin-parity J^π (parenthesis means tentative assignment from this work), and the associated spectroscopic factor C^2S for different values of r_0 and a_0. ZR stands for zero-range DWBA calculation while FR stands for finite-range calculation. In Refs. [16,17] the calculations are done using the zero-range approximation.

E (MeV)	$r_0 = 1.20$ fm, $a_0 = 0.70$ fm				$C^2S(ZR)$ (This work)	$r_0 = 1.25$ fm, $a_0 = 0.65$ fm	
	L	J^π	C^2S [16]	C^2S [17]		$C^2S(ZR)$ (This work)	$C^2S(FR)$ (This work)
0	1	$3/2^-$	1.3	1.03	1.60(11)	1.40(15)	1.50(17)
1.11	1	$1/2^-$	0.46	0.41	–	–	0.35(11)[a]
1.23	3	$5/2^-$	1.5	1.2	0.90(13)	0.80(11)	0.70(10)
1.71	3	$7/2^-$	2.7	1.8	2.70(10)	2.00(11)	2.50(14)
1.87	3	$7/2^-$	0.45	0.5	0.55(12)	0.40(10)	0.50(10)
3.35	3	$(7/2^-)$	–	–	2.00(8)	1.60(10)	2.40(15)
3.70	2	$(3/2^+)$	–	–	2.60(21)	1.90(25)	1.50(20)
3.94	0	$(1/2^+)$	–	–	0.80(6)	0.70(06)	0.70(10)

[a]Only four angles were used for the angular distribution, see text for more details.

the angles and the integration of this peak was possible only for $\theta_{lab} = 15$, 18, 21, and 24°. The L assignment for this state is therefore difficult to make. If we refer to previous work [16,17] a spin assignment of $1/2^-$, hence $L = 1$, was given with a spectroscopic factor of 0.46 and 0.41, respectively. As one can see in Fig. 5(b) the angular distribution of this state in our present work can be fitted with a $L = 1$ distribution. Assuming a $L = 1$ distribution, the finite-range DWBA calculation gives a spectroscopic factor of $C^2S = 0.35(11)$, which is compatible with previous work.

Even though the authors in Ref. [16] mention other states at higher excitation energy, the highest excitation energy for which angular distribution is given is 1.87 MeV. We report here three new angular distributions for the states at 3.35, 3.70, and 3.94 MeV as one can see in Fig. 5. The states at 3.70 MeV and 3.94 MeV exhibit a $L = 2$ and a $L = 0$ distribution, respectively, that probably comes from the inner sd shell of the nucleus. Concerning the state at 3.35 MeV, it corresponds to a $L = 3$ distribution for which we extract a spectroscopic factor of 2.40(15) in the finite-range calculation.

It is interesting to note that when looking at the result of the finite-range calculation, the $pf_{5/2}$ orbitals have a sum of 2.20(20) protons if we do not take into account our result for the $1/2^-$ state at 1.23 MeV. We get 2.55(23) if we take into account a spectroscopic factor of 0.35(11) for the $1/2^-$ state. The last result is quite large since one expects only two protons above the $\pi f_{7/2}$ orbital. In the case that 0.55 particles from the $\pi f_{7/2}$ orbital are situated in the $pf_{5/2}$ orbitals, we do not expect eight protons anymore in this $\pi f_{7/2}$ orbital but 7.45. Concerning the $7/2^-$ states, the sum of the spectroscopic factors gives 5.40 and the centroid of the $\pi f_{7/2}$ strength is

$$E(f_{7/2}) = \sum \frac{C^2S(7/2^-)E(7/2^-)}{C^2S(7/2^-)} = 2.45 \text{ MeV}. \quad (1)$$

This centroid corresponds to a lower limit since a part of the strength remains undetected. We have extracted only 5.40 over 8, which corresponds to 67% of the strength. As aforementioned, if one expects only 7.45, then it corresponds to 72% of the strength. We miss a part of the strength that must lie at higher excitation energy. Indeed the matching of the reaction was not sufficient in this experiment to populate $L = 3$ states at high energy. Figure 6 shows the evolution of the matching for the $(d,^3\text{He})$ reaction as a function of the total kinetic energy of the deuteron beam. The matching for the ground state with a 27 MeV deuteron beam is $0.76\hbar$. A deuteron beam around 75 to 90 MeV is indeed well matched for $L = 3$. The cross section for a $L = 3$ state calculated with Dwuck-5 drops very rapidly with the excitation energy in our case. It explains why we do not see other states above 4 MeV. In our experiment, considering the flat background in the spectrum (cf Fig. 3), we have determined that at least 130 counts are needed in a peak to be detected with a confidence level of 95%. We have translated this number of counts to a spectroscopic factor for a given excitation energy (cf Fig. 7). We can then define two different zones: the first one above the line corresponds to the detectable zone in our experiment while

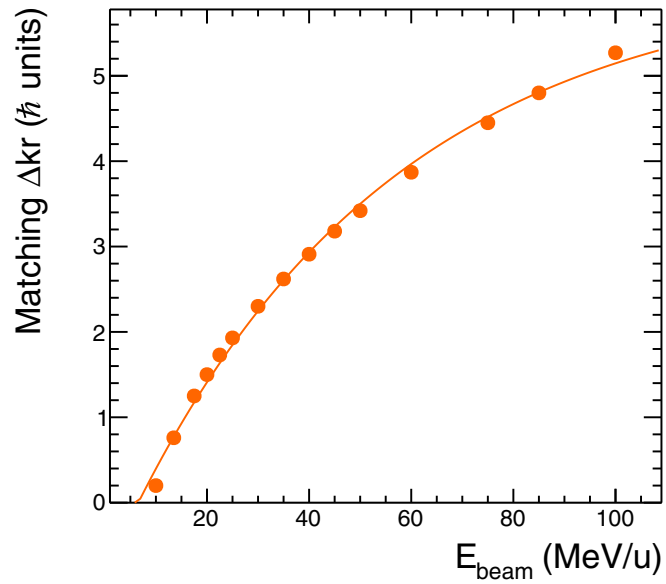

FIG. 6. Matching Δkr of the reaction to the ground state as a function of the total kinetic energy of the deuteron beam. The line corresponds to an exponential fit of the points.

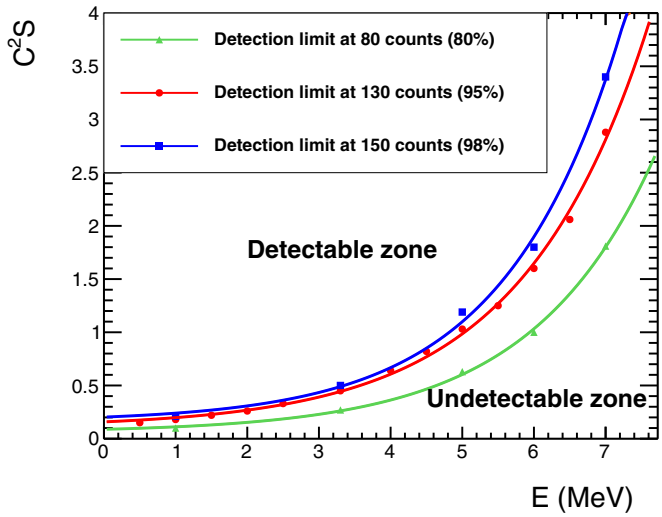

FIG. 7. Limit of spectroscopic factor as a function of the excitation energy. Two zones are defined: the detectable zone above the line and the undetectable one below the line.

the second one, below the line, corresponds to the undetectable zone. For instance, it means that if there was a $L = 3$ state at 5 MeV, the associated spectroscopic factor is necessarily lower than 1 because we did not see any peak at this energy in our experiment. The undetectable zone grows exponentially with the excitation energy. This is so because the cross section to populate a $L = 3$ state decreases exponentially as a function of the excitation energy. In this experiment, since we did not detect all of the strength we can only give a lower limit for the energy centroid.

It appears clearly that the population of $L = 3$ state in a neutron-rich region around nickel isotopes using a $(d,{}^3\mathrm{He})$ pick-up reaction where the Q values are very negative (-5.62 MeV in this case), needs to be performed around 40 MeV/u to be well matched and extract the maximum of the strength.

C. Shell-model calculation

Shell-model calculations within the $fpgd$ valence space and enacting the LNPS Hamiltonian [32] with further modifications to assure a proper evolution of the proton gap ($Z = 28$) between ^{68}Ni and ^{78}Ni [33] were carried out. The same Hamiltonian was used in our earlier study on ^{71}Cu [22] and in recent work on $^{69-73}$Cu [34]. Due to the large size of the configuration space, the calculations were truncated to $9p$-$9h$ across $Z = 28$ and $N = 40$. As one can see in Fig. 8, the calculation reproduces the $3/2^-$ as a ground state, however there is a factor of two difference in C^2S between the shell-model calculation and the extracted one using the finite-range DWBA calculation. The spectroscopic factor of the first $5/2^-$ excited state calculated at 1.25 MeV is satisfactorily reproduced while the main $7/2^-$ fragments are shifted up more than 1 MeV between the calculation and the experimental data.

In addition to the strength functions, calculations to determine the composition of the first low-lying states were

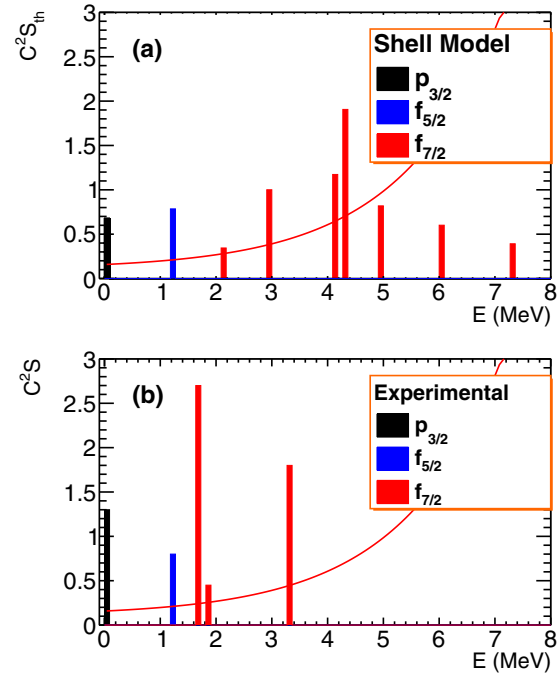

FIG. 8. States calculated from shell-model calculation with $C^2S_{th} > 0.3$ (a) compared to experimental data (b). The x axis represents the energy position of the states while the y axis shows the associated spectroscopic factor. The red line corresponds to the frontier between the detectable zone and the undetectable zone from Fig. 7. Peaks below this line cannot be measured in this experiment.

performed using the NATHAN code (see Table II). According to the shell-model calculation, the $3/2^-$ ground state corresponds largely to a single proton in the $p_{3/2}$ orbital. The dominant part of the $5/2^-$ state corresponds to a single proton in the $\pi f_{5/2}$ and is adequately located. The first $7/2^-$ state calculated at 1.86 MeV has a large part coming from the coupling $|2^+_\nu \otimes \pi p_{3/2}\rangle$ and has a large transition strength to the ground state of $B(E2) = 46\ e^2\mathrm{fm}^4$. However this state has a very low calculated spectroscopic factor and is not visible in Fig. 8. This state is remarkably close to the experimental level at 1.87 MeV where a strong $E2$ transition to the ground state has been observed with a measured $B(E2) = 77(12)\ e^2\mathrm{fm}^4$ [35]. The

TABLE II. Dominating components of the wave functions for the lowest calculated states in ^{69}Cu.

Energy (MeV)	J^π	Percentage	Composition
0	$3/2^-$	93%	$\|0^+_\nu \otimes \pi p_{3/2}\rangle$
1.25	$5/2^-$	37%	$\|0^+_\nu \otimes \pi f_{5/2}\rangle$
		20%	$\|2^+_\nu \otimes \pi p_{3/2}\rangle$
		16%	$\|2^+_\nu \otimes \pi f_{5/2}\rangle$
1.86	$7/2^-$	40%	$\|2^+_\nu \otimes \pi p_{3/2}\rangle$
		22%	$\|4^+_\nu \otimes \pi p_{3/2}\rangle$
		12%	$\|J^+_\nu \otimes \pi f^{-1}_{7/2}\rangle$
2.18	$7/2^-$	52%	$\|2^+_\nu \otimes \pi f_{5/2}\rangle$
		14%	$\|4^+_\nu \otimes \pi f_{5/2}\rangle$
		16%	$\|J^+_\nu \otimes \pi f^{-1}_{7/2}\rangle$

second calculated $7/2^-$ state at 2.18 MeV corresponds also to a coupling in particular with $\pi f_{5/2}$ but has a very low $B(E2)$ value (0.05 $e^2\text{fm}^4$) because the overlap with the $\pi p_{3/2}$ wave function of the ground state is small. Moreover, this state has a small calculated spectroscopic factor (0.34) and therefore does not match with the experimental level at 1.71 MeV. The first calculated $7/2^-$ state with large C^2S arises at 2.93 MeV and is situated 1.2 MeV above the 1.71 MeV experimental level. One should however note that the proton gap calculated in the shell model is 6.1 MeV on the monopole level and is reduced to 5.8 MeV when correlations are added. These values are in a good agreement with the experimental value extracted from masses (5.9 MeV) [36]. In addition, in the neighboring ^{71}Cu nucleus the position of the $f_{7/2}$ centroid seems to be well reproduced in the present shell model [22]. The correlation mechanism that could bring down the $f_{7/2}$ strength at $N = 40$ in the calculations is thus not understood. Interestingly, a similar problem has been encountered in the calculations for the $d_{5/2}$ strength in ^{67}Ni [37]. Thus, the fact that the $\pi f_{7/2}$ orbital is lower that the prediction implies that it should favor quadrupole collectivity between the $f_{7/2}$-$p_{3/2}$ proton orbitals. More investigations have to be performed in the future to pin down the single-particle strength in this neutron-rich region.

IV. CONCLUSION

The ^{70}Zn$(d,^3\text{He})^{69}$Cu transfer reaction was performed in direct kinematics and states up to excitation energies of 4 MeV were populated. From this work, there is no evidence of a doublet in the peak at 1.23 MeV, three new angular distributions have been measured, and spectroscopic factors were determined from comparison with finite-range DWBA calculations. Due to the poor matching of the reaction the higher-lying part of the $\pi f_{7/2}$ strength was not measured and a lower limit on the centroid of the strength is established at 2.45 MeV. A state-of-the-art shell-model calculation was performed and reproduces the $3/2^-$ and $5/2^-$ states but localizes the main fragments of the $7/2^-$ strength too high in energy.

ACKNOWLEDGMENTS

The continuous support of the staff of the Alto facility as well as the target laboratory staff as well as the CSNSM is gratefully acknowledged as well as the Romanian National Authority for Scientific Research, CNCS-UEFISCDI, Project No. PN-II-ID-PCE-2011-3-0487.

[1] M. Goeppert-Mayer, Phys. Rev. **75**, 1969 (1949).
[2] O. Haxel, J. H. D. Jensen, and H. E. Suess, Phys. Rev. **75**, 1766 (1949).
[3] O. Sorlin and M.-G. Porquet, Prog. Part. Nucl. Phys. **61**, 602 (2008).
[4] Z. Y. Xu *et al.*, Phys. Rev. Lett. **113**, 032505 (2014).
[5] M. Bernas, P. Dessagne, M. Langevin, J. Payet, F. Pougheon, and P. Roussel, Phys. Lett. B **113**, 279 (1982).
[6] O. Sorlin *et al.*, Phys. Rev. Lett. **88**, 092501 (2002).
[7] K. Langanke, J. Terasaki, F. Nowacki, D. J. Dean, and W. Nazarewicz, Phys. Rev. C **67**, 044314 (2003).
[8] W. F. Mueller *et al.*, Phys. Rev. C **61**, 054308 (2000).
[9] F. Recchia *et al.*, Phys. Rev. C **88**, 041302(R) (2013).
[10] F. Flavigny *et al.*, Phys. Rev. C **91**, 034310 (2015).
[11] S. Suchyta, S. N. Liddick, Y. Tsunoda, T. Otsuka, M. B. Bennett, A. Chemey, M. Honma, N. Larson, C. J. Prokop, S. J. Quinn, N. Shimizu, A. Simon, A. Spyrou, V. Tripathi, Y. Utsuno, and J. M. VonMoss, Phys. Rev. C **89**, 021301(R) (2014).
[12] A. Dijon *et al.*, Phys. Rev. C **85**, 031301(R) (2012).
[13] Y. Tsunoda, T. Otsuka, N. Shimizu, M. Honma, and Y. Utsuno, Phys. Rev. C **89**, 031301(R) (2014).
[14] S. Franchoo, M. Huyse, K. Kruglov, Y. Kudryavtsev, W. F. Mueller, R. Raabe, I. Reusen, P. VanDuppen, J. VanRoosbroeck, L. Vermeeren, A. Wohr, K. L. Kratz, B. Pfeiffer, and W. B. Walters, Phys. Rev. Lett. **81**, 3100 (1998).
[15] K. T. Flanagan *et al.*, Phys. Rev. Lett. **103**, 142501 (2009).
[16] B. Zeidman and J. A. Nolen, Phys. Rev. C **18**, 2122 (1978).
[17] F. Ajzenberg-Selove *et al.*, Phys. Rev. C **24**, 1762 (1981).
[18] R. J. Furnstahl and H.-W. Hammer, Phys. Lett. B **531**, 203 (2002).
[19] T. Duguet and G. Hagen, Phys. Rev. C **85**, 034330 (2012).
[20] J. P. Schiffer, C. R. Hoffman, B. P. Kay, J. A. Clark, C. M. Deibel, S. J. Freeman, A. M. Howard, A. J. Mitchell, P. D. Parker, D. K. Sharp, and J. S. Thomas, Phys. Rev. Lett. **108**, 022501 (2012).
[21] M. B. Tsang, J. Lee, and W. G. Lynch, Phys. Rev. Lett. **95**, 222501 (2005).
[22] P. Morfouace *et al.*, Phys. Lett. B **751**, 306 (2015).
[23] A. Matta *et al.*, J. Phys. G: Nucl. Part. Phys. **43**, 045113 (2016).
[24] J. E. Spencer and J. Sherman, Nucl. Instrum. Methods **49**, 181 (1967).
[25] R. G. Markham and R. G. Robertson, Nucl. Instrum. Methods **129**, 131 (1975).
[26] S. Benamara, N. deSereville, A. M. Laird, F. Hammache, I. Stefan, P. Roussel, S. Ancelin, M. Assie, A. Coc, I. Deloncle, S. P. Fox, J. Kiener, L. Lefebvre, A. Lefebvre-Schuhl, G. Mavilla, P. Morfouace, A. M. Sanchez-Benitez, L. Perrot, M. Sinha, V. Tatischeff, and M. Vandebrouck, Phys. Rev. C **89**, 065805 (2014).
[27] P. D. Kunz, computer code DWUCK4, University of Colorado (unpublished).
[28] W. W. Daehnick, J. D. Childs, and Z. Vrcelj, Phys. Rev. C **21**, 2253 (1980).
[29] C. Perey and F. Perey, At. Data Nucl. Data Tables **17**, 1 (1976).
[30] P. D. Kunz, computer code DWUCK5, University of Colorado (unpublished).
[31] I. Brida, S. C. Pieper, and R. B. Wiringa, Phys. Rev. C **84**, 024319 (2011).
[32] S. M. Lenzi, F. Nowacki, A. Poves, and K. Sieja, Phys. Rev. C **82**, 054301 (2010).
[33] K. Sieja and F. Nowacki, Phys. Rev. C **85**, 051301(R) (2012).
[34] E. Sahin *et al.*, Phys. Rev. C **91**, 034302 (2015).
[35] I. Stefanescu *et al.*, Phys. Rev. Lett. **100**, 112502 (2008).
[36] M. Wang, G. Audi, A. H. Wapstra, F. G. Kondev, M. MacCormick, X. Xu, and B. Pfeiffer, Chin. Phys. C **36**, 1603 (2012).
[37] J. Diriken *et al.*, Phys. Lett. B **736**, 533 (2014).